Chemical Engineering Science 216 (2020) 115535

Contents lists available at ScienceDirect

Chemical Engineering Science

journal homepage: www.elsevier.com/locate/ces

Effect of γ-Al_2O_3 characteristics on hydrogen production of Cu/γ-Al_2O_3 catalyst for steam reforming of dimethyl ether

Daesuk Kim [a], Byungchul Choi [b,*], Gyeongho Park [a], Kyungseok Lee [c], Dong-Weon Lee [b], Seunghun Jung [b]

[a] Graduate Student of Depart. of Mechanical Engineering, Chonnam National University, 77 Yongbong-ro, Bug-gu, Gwangju 61186, Republic of Korea
[b] School of Mechanical Engineering, Chonnam National University, 77 Yongbong-ro, Bug-gu, Gwangju 61186, Republic of Korea
[c] Automotive Research Center, Chonnam National University, 77 Yongbong-ro, Bug-gu, Gwangju 61186, Republic of Korea

HIGHLIGHTS

- Effect of kinds of γ-Al_2O_3 on H_2 production and stability of DME SR catalyst were studied.
- The optimum Cu content of the DME SR reaction was 5–10 wt%.
- H_2 was produced up to 72% on Cu10/γ-Al_2O_3 having BET(200) of 200 m^2/g.
- Cu10/γ-Al_2O_3(BET200 and 140) had the lower carbon deposition in the DME SR reaction.

GRAPHICAL ABSTRACT

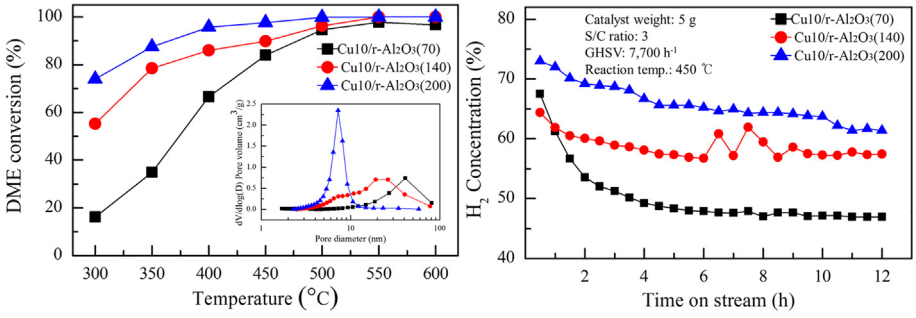

ARTICLE INFO

Article history:
Received 6 September 2019
Received in revised form 29 January 2020
Accepted 1 February 2020
Available online 3 February 2020

Keywords:
Hydrogen
Steam reforming catalyst
Copper
Alumina
Dimethyl ether

ABSTRACT

The objective of this study is to investigate the effect of the characteristics of γ-Al_2O_3 on hydrogen production and the stability of the Cu/γ-Al_2O_3 dimethyl ether steam reforming (SR) catalyst. Cu/γ-Al_2O_3 catalysts with various amounts of Cu were prepared by impregnation into γ-Al_2O_3 having different surface characteristics. The results demonstrate that the characteristics of the γ-Al_2O_3 support greatly affect the hydrogen production performance of the Cu-based/γ-Al_2O_3 DME SR catalysts, and that carbon deposition increased with the amount of CO and CH_4 that come from oxygenates (DME/MeOH) as coke precursors formed by DME hydrolysis reaction. The concentration of H_2 produced with Cu10/γ-Al_2O_3(200) was up to 72%, and it was higher than that of the other catalysts. The BET of Al_2O_3 affects different coke resistance and durability, in which the lowest BET shows severely deactivation and weak coke resistance compared to BET 140 and 200. Cu10/γ-Al_2O_3(200) and (140) catalysts were more durable and stable than Cu10/γ-Al_2O_3(70) due to lower carbon deposition on the catalyst surface.

© 2020 Elsevier Ltd. All rights reserved.

1. Introduction

Environmental pollution by fossil fuel combustion is driving the demand for alternative energy. Among several alternative fuels, hydrogen has attracted attention as a promising clean energy source (Durbin and Malardier-Jugroot, 2013, Hwang and Varma, 2014, González-Gil et al., 2016, Zhang et al., 2018c, Fedotov et al., 2018). Hydrogen has a higher energy density per unit weight than conventional fuels, as well as environmental advantages. Electric power units employing polymer electrolyte membrane fuel cells (PEMFCs) and hydrogen are considered as alternative power sources for electric vehicles (EV). Hydrogen as an automotive fuel is usually stored in a tank or produced on-board (Durbin and Malardier-Jugroot, 2013, Hwang and Varma, 2014, Inagaki et al., 2018). Among the hydrogen supply systems, the on-board production system is still

* Corresponding author.
E-mail address: bcchoi@jnu.ac.kr (B. Choi).

https://doi.org/10.1016/j.ces.2020.115535
0009-2509/© 2020 Elsevier Ltd. All rights reserved.

challenging because it requires a small and efficient fuel processor. In the fuel processor, hydrogen-rich gas for the PEMFC can be produced from hydrocarbon fuels, such as methane, or synthetic oxygenated organic compounds, such as methanol, ethanol, and dimethyl ether (DME) (Takeishi and Akaike, 2016). In contrast with hydrocarbons, DME is easy to handle due to its storage stability and transportability, and its physical characteristics that are similar to those of liquefied petroleum gas (LPG); thus, the existing LPG supply infrastructure can be utilized. In addition, DME has a high hydrogen mass fraction (13 wt%) and does not have any direct C-C bonds, and thus, can be reformed even at low temperatures. In this respect, DME is suitable as a hydrogen-rich gas carrier for on-board hydrogen production for vehicles. Hydrogen-rich gas can be produced from DME via partial oxidation, steam reforming (SR), and autothermal reforming (Deng et al., 2019, Pu et al., 2019). DME steam reforming has the highest yield of hydrogen among these methods and theoretically produces hydrogen-rich gas with less CO. Takeishi et al. (Takeishi and Suzuki, 2004, Takeishi and Akaike, 2016) reported that Cu/Al_2O_3 catalysts incorporating Zn and Pd were the best catalysts for the production of hydrogen while producing less CO in the temperature range of 250–350 °C. Semelsberger et al. (2006) reported that the most active catalyst was Cu-Zn/γ-Al_2O_3, affording a hydrogen yield of 89% at 400 °C. However, in practice, when catalysts are prepared as pellets or honeycombs, the reaction temperature may be higher than that in the laboratory-scale experiments using the powder catalyst.

Steam reforming of DME can be carried out at 250–500 °C, and generally proceeds via two reaction processes. The primary global SR reaction of DME (Eq. (1)) involves a combination of DME hydrolysis (Eq. (2)) to methanol over a solid-acid catalyst and steam reforming of methanol (Eq. (3)) to hydrogen and CO_2 over a metallic catalyst (Fukunaga et al., 2008, Oar-Arteta et al., 2016a, Oar-Arteta et al., 2016b). Methanol steam reforming occurs at temperatures of 200–300 °C; however, the hydrolysis of DME to methanol occurs at a relatively higher temperature (300–400 °C) (Elewuwa and Makkawi, 2015). The water gas shift reaction (Eq. (4)) also occurs during the DME steam reforming reaction. In addition, non-desirable side reactions (Eqs. (5)–(9)) can occur depending on the reaction conditions and nature of the catalyst (Elewuwa and Makkawi, 2015, Hwang and Varma, 2014, Ledesma et al., 2011).

DME steam reforming: $CH_3OCH_3 + 3H_2O \rightarrow 6H_2 + 2CO_2$ (1)

DME hydrolysis: $CH_3OCH_3 + H_2O \rightarrow 2CH_3OH$ (2)

MeOH steam reforming: $CH_3OH + H_2O \rightarrow 3H_2 + CO_2$ (3)

Water gas shift: $CO + H_2O \rightarrow CO_2 + H_2$ (4)

DME decomposition: $CH_3OCH_3 \rightarrow CH_4 + H_2 + CO$ (5)

Direct CO_2 formation: $CH_3OCH_3 + H_2O \rightarrow CH_4 + CO_2 + 2H_2$ (6)

MeOH decomposition: $CH_3OH \rightarrow 2H_2 + CO$ (7)

Methanation: $CO + 3H_2 \rightarrow CH_4 + H_2O$ (8)

Boudouard reaction: $2CO \rightarrow C + CO_2$ (9)

SR DME catalysts must possess acidic and metallic functionality for DME hydrolysis and steam reforming of methanol, respectively. Metallic copper oxides loaded onto an alumina support are quite often used as bifunctional catalysts for the steam reforming of DME. To achieve the metallic function, Cu-based/γ-Al_2O_3 catalysts are applied for the steam reforming of methanol or DME, and Cu-spinel oxides or alloys are also used for prevention of Cu sintering (Ereña et al., 2013, Faungnawakij et al., 2008, Gayubo et al., 2014, Oar-Arteta et al., 2016b). The Cu species in the $CuFe_2O_4$ spinel structure exhibit not only high activity, but also good stability in DME SR above 300 °C, but a high calcination temperature (900 °C) is required (Faungnawakij et al., 2008, Oar-Arteta et al., 2014). To improve the thermal stability of Cu-based catalysts, several secondary components have been selected and added to the Cu/γ-Al_2O_3/Al catalyst. The effects of Pd, Ni, Fe, Co, and Zn loading and the effects of the chemical state of these species on the performance of the catalysts have been extensively investigated (Jiao et al., 2016, Ledesma et al., 2011, Mansouri et al., 2014, Oar-Arteta et al., 2014, Vizcaíno et al., 2007).

On the other hand, γ-Al_2O_3 and zeolites, used as supports to confer the acidic function, can act as Lewis acid sites for DME hydrolysis. The properties of the γ-Al_2O_3 support vary with the synthesis conditions (Melkozerova et al., 2018). Zeolites, such as HZSM-5 (Gayubo et al., 2014, Oar-Arteta et al., 2014) and mordenite (Fukunaga et al., 2008, Inagaki et al., 2018, Vicente et al., 2013) promote DME hydrolysis at lower temperatures compared to the alumina support. However, due to the strong acid sites, zeolites can induce coke formation and the production of hydrocarbons, leading to deactivation. Alumina is amorphous and occurs as various phases with different characteristics depending on the precursor materials and preparation method. The calcination temperature of the alumina precursor effects phase transformation from the gamma to alpha phase, where the latter has a stable hexagonal corundum structure. In this phase-transformation during calcination, the coordination state of the internal Al ions changes. These phase changes of alumina can affect the steam reforming of DME. In our previous work, the reaction characteristics of a Cu-based/γ-Al_2O_3 catalyst loaded on a commercial alumina support were studied, with focus on the effects of additives (Ni and Ce) and the support (mordenite). We also determined the most suitable reaction conditions for the DME SR catalysts, such as the H_2O/DME ratios, operative temperature range, and space velocity (SV). The optimal Cu content was found to be 10 wt% (Kim et al., 2017, Park et al., 2011a, Park et al., 2011b, Park et al., 2012). And about a coke phenomenon, which could be the oxygenates (DME/MeOH). The role of these oxygenates as coke precursors by means of methoxy ions in DME steam reforming has been reported in literature. Thus far, many studies have investigated the effect of the main catalyst, additives, and acidic characteristics of the support on the DME SR reaction. However, studies on the effect of the characteristics of alumina on the catalyst performance in DME steam reforming are insufficient.

The main purpose of this study is to investigate the effect of the characteristics of γ-Al_2O_3 on hydrogen production and the stability of the Cu-based/γ-Al_2O_3 DME steam reforming catalyst. For this purpose, Cu/γ-Al_2O_3 catalysts with different amounts of copper are prepared by impregnation using commercial γ-Al_2O_3 with various surface characteristics. The catalysts are characterized by N_2-isotherm, X-ray diffraction (XRD), X-ray photoelectron spectroscopy (XPS), and nuclear magnetic resonance (NMR) analyses. Further analysis of the long-term stability is conducted through time-on-stream (TOS) and thermal gravimetric analyses (TGA).

2. Experimental

2.1. Catalysts preparation

The Cu/γ-Al_2O_3 catalysts were prepared by impregnation and the detailed specifications of the Cu precursor and the γ-Al_2O_3 used

in the preparation are presented in Table 1. γ-Al_2O_3 was added to distilled water at 60 °C, and the mixture was stirred for 30 min. The Cu precursor was then added and stirred for 2 h. The resultant solution was evaporated to dryness for 12 h under air atmosphere at 100 °C, followed by milling of the residue. The catalyst powder was calcined at 500 °C for 2 h at a heating rate of 2 °C/min. Finally, the powder was pressurized at 250 bar to form a pellet with a diameter of 3 mm, height of 5 mm, and weight of 0.03 g per pellet. The prepared Cu/γ-Al_2O_3 catalysts are denoted as CuX/γ-Al_2O_3(Y), where X corresponds to the Cu concentration (5, 10, 15, and 30 wt%) and Y indicates the specific surface area of γ-Al_2O_3 (70, 140, and 200 m^2 g^{-1}), as analyzed by the Brunauer-Emmett-Teller (BET) method.

2.2. Experimental apparatus

Fig. 1 illustrates the experimental setup for DME steam reforming. The experiment was conducted in a quartz fixed-bed reactor with a diameter of 20 mm and length of 300 mm under atmospheric pressure. The temperature of the reactor was controlled and maintained by an electric furnace. The supply flow rate for DME was adjusted using a mass flow controller (MFC), and the H_2O feed was adjusted using a syringe pump·H_2O was vaporized by passing through a vaporizer maintained at 300 °C and then supplied to the DME reforming reactor. The steam in the outlet gas of the reformer was eliminated by a H_2O-trap maintained at −10 °C prior to gas analysis. After eliminating the steam, the gas was sampled using a syringe (40 mL) and supplied to a gas chromatograph (GC, HP 6890) with a thermal conductivity detector (TCD). After trapping the produced water at 0 °C, unreacted DME could be dissolved in the trap because the solubility of DME in water at 20 °C is approximately 71 g/L (Dimethyl Ether, 2019). However, this phenomenon would not severely affect the catalytic performance during the DME SR reaction. A packed column (Shin Carbon ST, Restek) was used to separate H_2, CO, CO_2, and CH_4. A capillary column (molecular sieves 5A, Agilent) was used to separate DME and CH_4 and a flame ionization detector (FID) was used in the analysis.

2.3. Experimental procedure

Table 2 shows the experimental conditions for evaluating the performance of the DME SR catalysts. The reforming reaction temperature was in the range of 300–600 °C and a gas hourly space velocity (GHSV) of 7700 h^{-1} was employed. The steam-to-carbon (*S/C*) ratio based on the molar mass was set to 3, which is the experimental value used in our previous studies (Kim et al., 2017). The *S/C* ratio is one of the main parameters in the SR reaction and is mainly set to a higher ratio than the stoichiometric ratio to prevent carbon deposition. All reforming catalysts were reduced under hydrogen atmosphere (500 mL min^{-1}, 10% H_2/N_2) at 500 °C for 1 h before the experiment. After the reduction treatment, only water vapor was supplied to the reactor for 5 min. This experiment was carried out without a carrier gas to simulate the actual SR reaction conditions, and only DME was supplied after stabilization of the internal temperature of the reactor. The experiment was repeated four times at a given temperature while increasing the temperature in increments. The reason for exclusion of the initial measurement is that the reactants of the SR reaction could not fill the volume of the reactor and H_2O trap. Before the SR reaction, the catalyst was treated with H_2/N_2 (10% balance); thereafter, the predetermined reaction gases were introduced. The residual gases were entirely exhausted from the reactor for 20 min and carried to the GC. Therefore, the initial experiment was excluded to estimate the average conversion because H_2/N_2 could remain in the reactor. The fluctuation of the data was within 1% of the average value. These experimental conditions were selected for determination of the actual optimum Cu content prior to analyzing the effect of the characteristics of γ-Al_2O_3 on the DME SR performance of the catalyst.

Table 1
Precursor of various catalysts and supports.

Metal	Precursor	Manufacturer	Characterization
Cu	$Cu(NO_3)_2$ $2.5H_2O$	Sigma Aldrich	–
γ-Al_2O_3 (70)	–	Alfa Aesar	BET 80–120 m^2/g APS* 3 μm
γ-Al_2O_3 (140)	–	Alfa Aesar	BET 100–200 m^2/g APS 20 nm
γ-Al_2O_3 (200)	–	Alfa Aesar	BET 200 m^2/g APS 32–63 μm

*APS: average particle size.

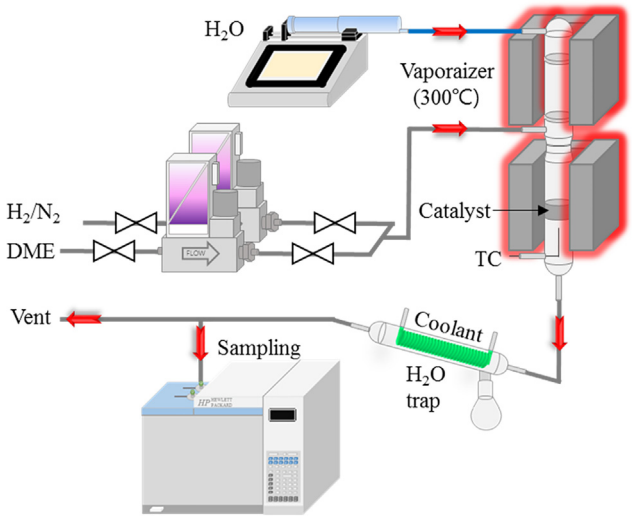

Fig. 1. Experimental apparatus for reaction test of the reforming.

Table 2
Experimental conditions for the performance test of the reforming catalysts.

Parameter	Condition
Temperature condition	Steady state
Analysis temperature (°C)	300–600
DME flow rate (mL/min)	50
H_2O flow rate (mL/min)	0.248
Vaporizer temperature (°C)	300
Catalysts weight (g)	5

2.4. Characterization methods

The reducibility of the catalysts was analyzed by temperature programmed reduction with hydrogen (H_2-TPR) on a BEL-CAT (BEL) apparatus. Prior to H_2-TPR, each catalyst (0.05 g) was pretreated under argon at 500 °C. H_2-TPR was conducted in the range of 50–700 °C under 5% H_2/Ar at a flow rate of 30 mL min^{-1}. X-ray photoelectron spectroscopy (XPS) was used for surface chemical analysis of the catalyst by employing a K-Alpha+ (Thermo Fisher Scientific) apparatus equipped with an Al K-α X-ray monochromator. X-ray diffraction (XRD) was used to analyze the crystallinity of the catalyst, and an EMPYREAN (PANalytical) instrument equipped with a Cu-Kα X-ray source (40 kV, 30 mA, λ = 1.5406 Å) was used for the analysis. The crystallite size of CuO was calculated using the Scherrer equation. Nitrogen adsorption-desorption isotherms were

obtained at − 196 °C with an ASAP2020 (Micromeriticis) instrument. The specific surface area was based on the Brunauer-Emmett-Teller (BET) method. The pore size distributions were calculated from the desorption branch using the Barrett-Joyner-Halenda (BJH) method. The micropore volume was determined using the t-plot method. Solid-state ^{27}Al MAS-NMR (nuclear magnetic resonance) experiments were conducted with an EZCR400 (JEOL) equipment. An external magnetic field of 9.4 T and operating frequency of 104.17 MHz were employed for the experiments, which were conducted on a 400 MHz spectrometer at room temperature. Thermogravimetric analysis (TGA) was conducted on a TGA2 (Mettler Toledo) equipment to analyze the oxidation characteristics and measure the degree of carbon deposition on the catalyst. The mass reduction of the catalyst was measured in the range of 300–900 °C (heating rate of 10 °C/min) with an air flow rate of 50 mL/min.

3. Results and discussion

3.1. Determination of the optimum Cu content

Fig. 2 shows the DME conversion obtained with various Cu contents. As shown in Fig. 2(a), for γ-Al_2O_3(70), the DME conversion increased rapidly at 350 °C and >80% of the DME was converted at 450 °C. The DME conversion obtained with the Cu 5 wt% and Cu 30 wt% catalysts differed by 10.56% at 450 °C. Fig. 2(b) presents the DME conversion achieved with γ-Al_2O_3(140) loaded with various Cu contents. In this case, 80% conversion was achieved at 350 °C, which is 100 °C lower than the temperature required for similar conversion with γ-Al_2O_3(70). In the temperature range of 300–350 °C, the conversion increased rapidly, and the DME conversion increased as the Cu content decreased. Above 500 °C, the tendency was reversed relative to the results obtained in the previous temperature range. This reversal of the DME conversion above 500 °C was also observed in the case of γ-Al_2O_3(70). This is attributed to a reduction in the number of active sites due to agglomeration of Cu. The DME conversion decreased significantly due to diminution of the absolute amounts of active sites when the Cu content was low. Fig. 2(c) shows the DME conversion obtained with CuX/γ-Al_2O_3(200), for which the DME conversion was much higher than that of γ-Al_2O_3(70) and (140). The DME conversions of CuX/γ-Al_2O_3(70) were lower that other CuX/γ-Al_2O_3(140) and (200) below 500 °C. In this time, DME/MeOH as coke precursors may be able to produce. The DME conversion decreased markedly when the Cu loading exceeded 15 wt% below 450 °C. The DME conversion achieved using the three types of Cu10/γ-Al_2O_3 catalysts reached 100% at a reaction temperature of 500 °C.

Fig. 3 depicts a comparison of the exhaust emission from the reformer treated with the CuX/γ-Al_2O_3 (70), (140), and (200) catalysts. In Fig. 3(a-1), the markers on the graph, such as group (a), (b), and (c) indicate γ-Al_2O_3(70), γ-Al_2O_3(140), and γ-Al_2O_3(200), respectively, and (1)–(4) indicate the Cu content (5, 10, 20, and 30 wt%). Fig. 3(a-1) depicts a decrease in the hydrogen concentration at temperatures exceeding 500 °C. Fig. 3(a-2) indicates that the maximum hydrogen concentration was 62% at 550 °C. For group (a) in Fig. 3, the CO and CH_4 production were higher than group (b) and (c), and the CH_4 concentration increased with an increase in the Cu content. In the DME steam reforming reaction, CH_4 can be produced by the DME decomposition (Eq. (5)) and the CO methanation (Eq. (8)) or CO_2 methanation. As depicted in Fig. 2, when the DME conversion remained low below 500 °C; DME/MeOH as coke precursors may be able to produce, and DME/MeOH continuously produced the CO and CH_4. Over 500 °C; it was determined that the CH_4 was derived from the DME decomposition (Eq. (5)) based on the decrease in the H_2 production and

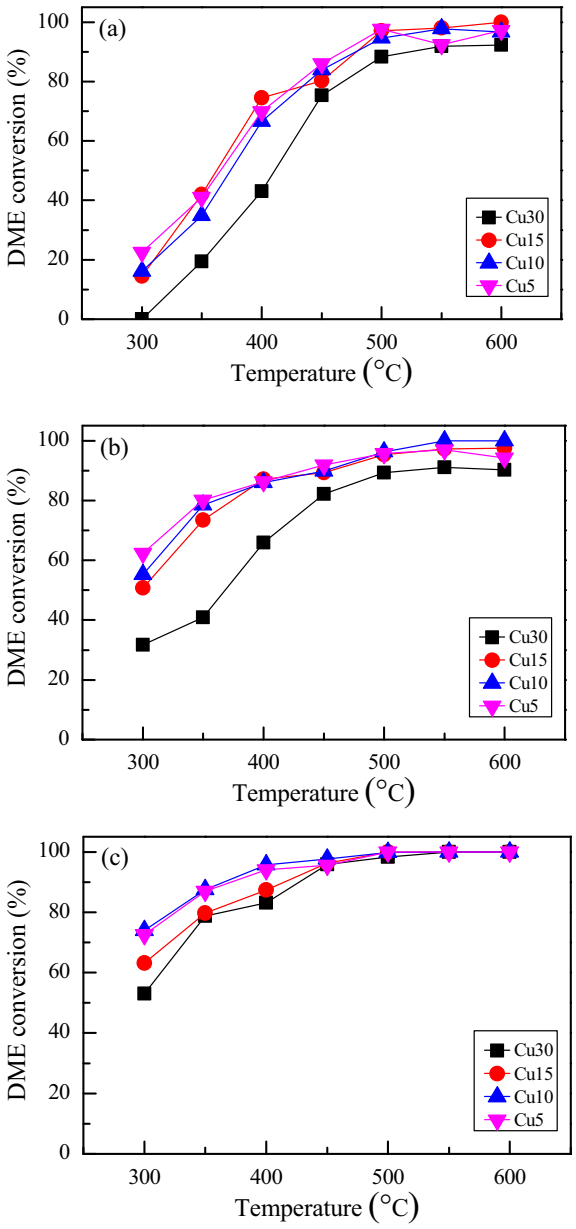

Fig. 2. DME Conversion of CuX/γ-Al_2O_3 catalysts. (a) CuX/γ-Al_2O_3(70), (b) CuX/γ-Al_2O_3(140) and (c) CuX/γ-Al_2O_3(200). Reforming reaction conditions: S/C ratio: 3, catalyst weight: 5 g, GHSV: 7700 h^{-1}.

the increased CH_4 formation. The CO and CO_2 methanations also contributed to the increased CH_4 production because CO and H_2 were simultaneously reduced above 500 °C, as illustrated in Fig. 3(a-1) (Chen et al., 2017, Deng et al., 2015, Deng et al., 2019). Moreover, CO_2 is directly formed (Eq. (6)) at temperatures above 500 °C and the methane and CO_2 production increases simultaneously. Fig. 3(b) indicates that the concentration of CO_2 detected below 450 °C increased as the content of Cu in the catalyst decreased. The concentration of CO_2 and methane increased above 450 °C. Above 450 °C, the CO decreased, and CH_4 and CO_2 increased; however, the H_2 production did not change significantly. This is attributed to the DME decomposition, after which the WGS reaction may occur to produce CO_2 and H_2. As depicted in Fig. 3, group (c) produced a higher hydrogen and lower CO and methane concentration at all temperatures in comparison with groups (a) and (b). The hydrogen production achieved with

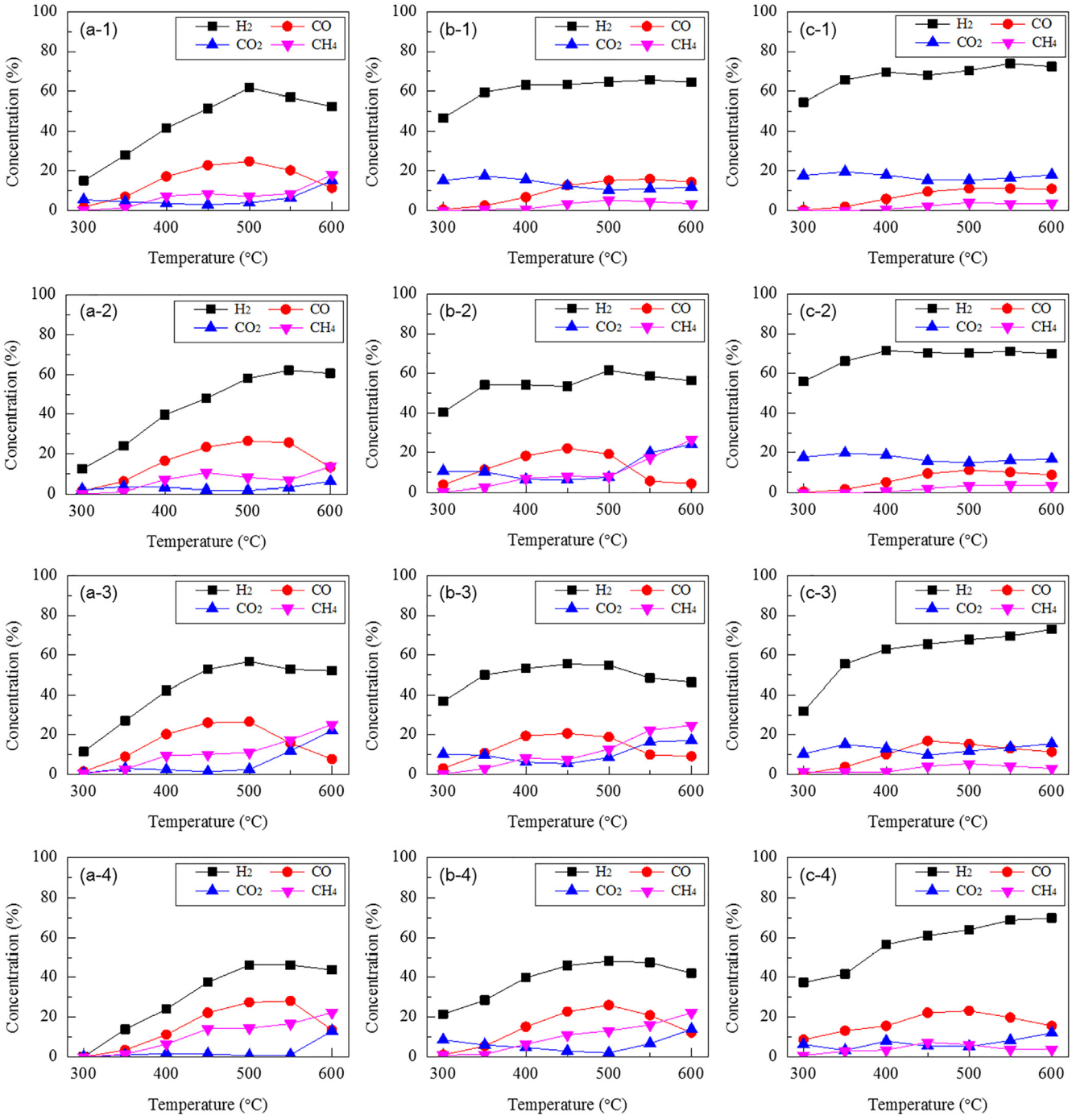

Fig. 3. DME steam reforming performance of CuX/γ-Al_2O_3 catalysts. (Alphabet-number: (a) γ-Al_2O_3(70), (b) γ-Al_2O_3(140) and (c) γ-Al_2O_3(200) – (1) Cu 5 wt%, (2) Cu 10 wt%, (3) Cu 15 wt% and (4) Cu 30 wt%). Reforming reaction conditions: S/C ratio: 3, catalyst weight: 5 g, GHSV: 7,700 h^{-1}.

Cu10/γ-Al_2O_3(200) was as high as 72%, which is higher than that of the Cu10/γ-Al_2O_3(70 and 140) catalysts.

Based on the results in Fig. 2 and Fig. 3, the optimal Cu content of the catalyst is less than 10 wt%. The effect of γ-Al_2O_3 on the DME SR reaction was investigated by characterization of the catalysts. The higher the surface area of the support, the more Cu that can be impregnated into the pore. Within the limits of the Cu content that the support can contain, Cu exists in the form of CuO species. Above this limiting amount, Cu is agglomerated to produce bulk Cu and the reforming performance of the catalyst is reduced (Park et al., 2011a, Park et al., 2011b, Park et al., 2012). The catalysts impregnated with 5 wt% and 10 wt% Cu on all supports exhibited similar reforming performance. Impregnation of the supports with lower Cu contents was found to be effective under all temperature conditions. The maximum H_2 production was obtained with the Cu 10 wt% catalyst and γ-Al_2O_3(200) support. Therefore, the 10 wt% Cu catalyst was selected for characterization in the DME SR reaction.

3.2. Characterization of catalyst

3.2.1. BET analysis

Table 3 shows the BET specific surface area, BJH pore volume, and mean pore diameter of the pure γ-Al_2O_3 and steam reforming

catalysts. The specific surface area of the catalysts, except for that of γ-Al_2O_3(70), was within the range of the specifications indicated in Table 1. The aluminum sites in γ-Al_2O_3 can generally provide three types of coordination, i.e., tetrahedral (AlO_4), pentahedral (AlO_5), and octahedral (AlO_6). The pure γ-Al_2O_3 supports and the Cu10/γ-Al_2O_3 catalysts showed a similar trend, where the mean pore diameter and micropore volume decreased with an increase in the BET surface area of γ-Al_2O_3. All of the SR catalysts were calcined at 500 °C, as mentioned in Section 2.1. The total pore volume of Cu10/γ-Al_2O_3(70) increased after Cu impregnation. It is assumed that the boehmite in γ-Al_2O_3(70) (see the XRD pattern in Fig. 6) was activated at the calcination temperature, indicating the development of pores.

Fig. 4 presents the pore size distribution of γ-Al_2O_3 and Cu/γ-Al_2O_3. γ-Al_2O_3(70) was mainly composed of 40 nm pores and γ-Al_2O_3(140) was mainly composed of 20 nm pores, but with some 7 nm pores. γ-Al_2O_3(200) was mainly composed of 7 nm pores. This pore distribution shows that all three types of γ-Al_2O_3 exhibit mesoporous properties, which is a general characteristic of γ-Al_2O_3. The pore size distribution of Cu-impregnated γ-Al_2O_3 is shown in Fig. 4(b). Thus, no change in the pore size distribution due to Cu impregnation was observed. As shown in Figs. 2 and 3, a higher specific surface area of γ-Al_2O_3 was associated with better DME SR performance (Park et al., 2012). This improvement is attributed to the effect of the surface area of the support on the degree of dispersion of the loaded copper nanoparticles.

3.2.2. H_2-TPR analysis

Fig. 5 depicts the H_2-TPR reducibility data for the catalysts with the same Cu content (10 wt%) impregnated into the different γ-Al_2O_3 supports. The results can be divided into three zones based on the temperature range: <280 °C, 280–500 °C, and >500 °C. The first temperature range (<280 °C) is ascribed to the non-spinel CuO species, the second temperature range (280–500 °C) to spinel-type Cu species, and the third temperature range (>500 °C) to hardly-reducible spinel-type Cu species (Qin et al., 2017). Table 4 presents a quantitative evaluation (H_2 consumption and Cu-Al spinel phase ratio) of each peak in the TPR profiles. The Cu-Al spinel phase ratio was calculated based on the molar ratio of Cu in the Cu-Al spinel phase to the total Cu, as derived from H_2-TPR. The first peak at 210 °C is attributed to highly dispersed non-spinel copper oxide (CuO) (Lei et al., 2018, Manzoli et al., 2005, Thyssen et al., 2015, Zhang et al., 2018a,b,c). Cu10/γ-Al_2O_3(200) exhibited a second peak in the non-spinel temperature range. The H_2 consumption at 210 °C was 0.146, 0.675, and 1.979 mmol g^{-1}, respectively, for Cu10/γ-Al_2O_3 (70), (140), and (200). Non-spinel CuO species can initiate steam reforming at a lower temperature, after which $CuAl_2O_4$ gradually releases active copper during the reaction. Therefore, as depicted in Figs. 2 and 3, the DME conversion and H_2 formation with Cu10/γ-Al_2O_3(200) was higher than with the other catalysts. A second peak was observed at 330 and 378 °C for Cu10/γ-Al_2O_3 (70) and (140) in the range of the spinel-type Cu species, respectively. In the DME reforming reaction, active Cu species can be released from the Cu-Al spinel structure. The spinel content in

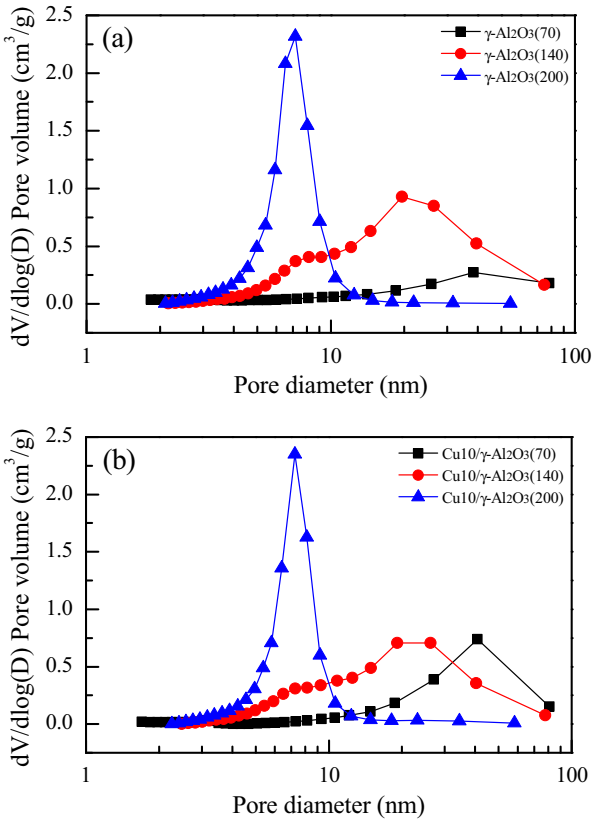

Fig. 4. Pore size distributions of the (a) γ-Al_2O_3 and (b) Cu10/γ-Al_2O_3.

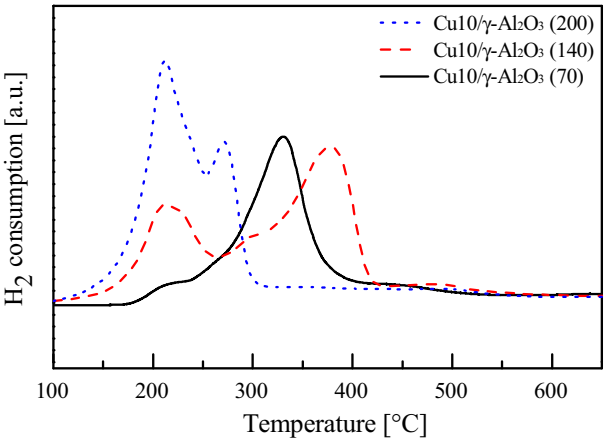

Fig. 5. H_2-TPR profiles of Cu10/γ-Al_2O_3 catalysts.

the Cu10/γ-Al_2O_3 (70), (140), and (200) catalysts was 5.2, 64.4, and 16.0%, respectively (Table 4). This peak is attributed to the strong interaction between Cu and the support. The Cu species

Table 3
BET surface area, mean pore diameter and pore volume of γ-Al_2O_3 supports and Cu10/γ-Al_2O_3 catalysts.

Catalysts	BET specific surface area (m^2/g)	Mean pore diameter (nm)	Total pore volume (cm^3/g)	Micropore volume (cm^3/g)
γ-Al_2O_3(70)	73.85	17.145	0.275	0.01344
γ-Al_2O_3(140)	141.65	18.193	0.712	0.00642
γ-Al_2O_3(200)	200.64	7.391	0.466	0.00067
Cu10/γ-Al_2O_3(70)	70.10	29.283	0.407	0.01455
Cu10/γ-Al_2O_3(140)	112.94	17.354	0.536	0.00764
Cu10/γ-Al_2O_3(200)	174.18	8.027	0.427	0.00468

Table 4
Characteristics of the catalysts from TPR spectra.

Catalyst	Peak Temperature (°C)	H_2 consumption (mmol/g)	Non-spinel (<280 °C)	Spinel (280–500 °C)	Hardly-reducible spinel (>500 °C)
Cu10/γ-Al_2O_3(70)	212.5	0.146	8.3	85.2	6.5
	330.2	1.496			
Cu10/γ-Al_2O_3(140)	211.4	0.657	33.2	64.4	2.4
	377.9	1.333			
Cu10/γ-Al_2O_3(200)	211.7	1.979	82.5	16.0	1.7
	257.8	0.328			

contained in the Cu-Al spinel structure contribute to the DME conversion and H_2 formation at higher temperatures (Tanaka et al., 2005). Therefore, it was found that H_2 formation by the DME SR is significantly affected by the Cu-Al spinel structure.

3.2.3. XRD analysis

Fig. 6 presents the diffraction patterns of γ-Al_2O_3 and the Cu-impregnated catalysts. Peaks attributable to γ-Al_2O_3 and peaks corresponding to boehmite at 14.5°, 28.19°, 38.41°, 49.01°, 55.2°, 64.05° and 72.06° were observed in the profile of γ-Al_2O_3(70) (Lei et al., 2018, Manzoli et al., 2005, Turco et al., 2007). The presence of boehmite is considered as the result of insufficient calcination during the synthesis of γ-Al_2O_3. The boehmite peaks of γ-Al_2O_3(70) disappeared in the profile of the Cu10/γ-Al_2O_3(70) catalyst that was calcined at 500 °C. In the case of the Cu-impregnated catalysts, diffraction peaks attributable to CuO (2θ = 35.5 and 38.7°) and Cu_2O (2θ = 61.85°) were observed. The average size of the CuO crystallites in Cu 10/γ- Al_2O_3 (70), Cu 10/γ- Al_2O_3 (140), and Cu 10/γ-Al_2O_3 (200) was 12.91, 14.26, and 7.9 nm, respectively, as calculated by applying the Scherrer equation. Comparison of Cu10/γ- Al_2O_3 (70) and Cu10/γ- Al_2O_3 (200) shows that the larger the BET surface area of the support, the smaller the crystallite size. Comparison of Cu10/γ-Al_2O_3 (140) and Cu10/γ- Al_2O_3 (200) suggests that the larger the APS(average particle size) of the support, the smaller the crystallite size.

3.2.4. XPS analysis

The valence states of Cu in the Cu-impregnated catalysts were determined by XPS analysis, as shown in Fig. 7. The spectra of the Cu 2p core level at binding energies between 965 and 925 eV indicate the valence states of the Cu species. The peaks at binding energies in the range of 952–955 eV correspond to Cu $2p_{1/2}$ and the peaks at binding energies from 932 to 938 eV correspond to Cu $2p_{3/2}$, attributed to Cu_2O (at 933 eV) and CuO (at 933.5 eV), i.e., Cu in the + 1 and + 2 valence states, respectively (Fan et al., 2016, Lei et al., 2018, Tanaka et al., 2005). The satellite peaks at 943 and 963 eV are typical of CuO. The XRD data in Fig. 6 confirm the presence of Cu_2O and CuO, consistent with the XPS data. The number of counts per second (cps) for Cu^{2+} in Cu10/γ- Al_2O_3 (70), (140), and (200) was 9361.1, 22250.2, and 52571.3, and the number of cps for Cu^+ was 13153.6, 23993.8, and 13656.6, respectively. The relative height and area of the XPS peaks indicate the quantitative frequency of Cu exposed on the catalyst surface. This implies that more Cu is exposed on the catalyst surface when a support with a large specific surface area is used. Therefore, as indicated by the TPR results (Fig. 5), large-area Cu^{2+} resulted in greater H_2 consumption. As shown in Fig. 7, the peaks at binding energies from 932 to 938 eV in the profile of the Cu10/γ-Al_2O_3(200) catalyst were more intense than those of the other catalysts; therefore, the SR performance of Cu10/γ-Al_2O_3(200) is expected to be superior to that of the other catalysts.

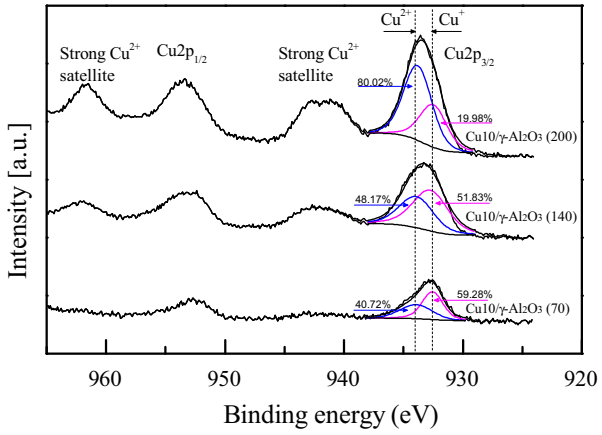

Fig. 7. XPS spectra of Cu10/γ-Al_2O_3 catalysts.

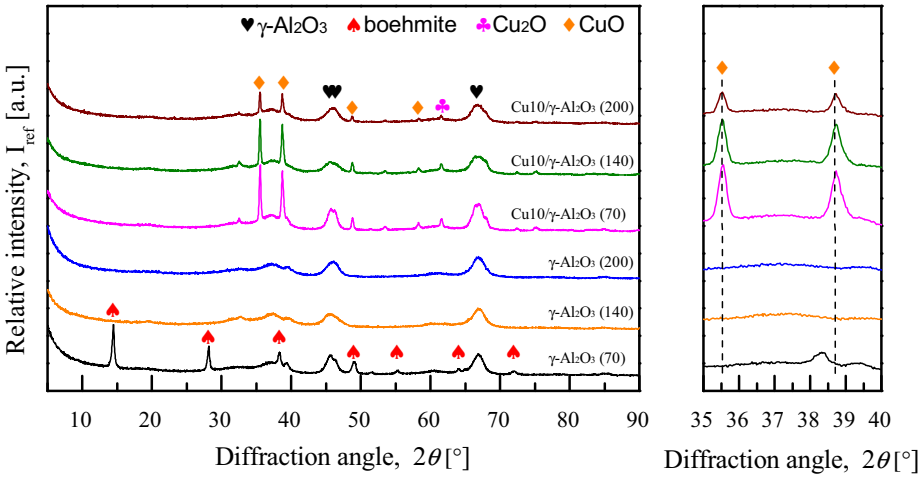

Fig. 6. XRD patterns of Cu10/γ-Al_2O_3 and γ-Al_2O_3. (♥) γ-Al_2O_3, (♠) boehmite, (♣) Cu_2O and (♦) CuO.

3.2.5. Analysis of ^{27}Al MAS NMR spectroscopy

The coordination environment of Al in the Cu10/γ-Al_2O_3 catalyst was evaluated by solid-state ^{27}Al MAS NMR spectroscopy (Fig. 8). Generally, the coordination ratio of tetrahedral (AlO_4):octahedral (AlO_6) Al in the γ-Al_2O_3 support is 7:3; pentahedral (AlO_5) coordination may occur depending on the manufacturing method (O'Dell et al., 2007, Zhang et al., 1995). The Al coordination in the Cu10/γ-Al_2O_3(70), (140), and (200) catalysts and γ-Al_2O_3 was compared for the pristine samples and those after calcination at 500 °C. Tetrahedral (AlO_4, 73 ppm), pentahedral (AlO_5, 35 ppm), and octahedral (AlO_6, 13 ppm) coordination of Al with oxygen was observed in the Cu10/γ-Al_2O_3 catalysts, and overall, octahedral coordination appeared to be dominant. For the γ-Al_2O_3(200) support, pentahedral coordination was present in the pristine sample, and after calcination at 500 °C it was confirmed that a small amount of additional pentahedral coordination was present. The peak of the pentahedrally coordinated species disappeared upon Cu impregnation (Kwak et al., 2007, Deng et al., 2015). During Cu impregnation, Cu bonds to the pentahedral site of Al, which changes the coordination to octahedral. Thus, it can be assumed that the octahedral Cu-O-Al structure was produced by the above process. Cu-O-Al (octahedral) was formed due to the strong interaction between Cu and γ-Al_2O_3 (Deng et al., 2015, Samain et al., 2014).

3.3. Durability of SR catalysts

3.3.1. TGA analysis

Fig. 9 shows the TGA data used to determine the amount of carbon accumulated in the catalyst after the DME SR for 10 h at 450 °C over the Cu10/γ-Al_2O_3 catalysts. TGA was performed on the reduced-catalyst and the SR catalysts at the outlet (bot), middle (mid), and inlet (top) positions in the mixture flow direction. The carbon deposition characteristics of the catalysts were determined by comparison of the difference in the TGA data for the used and fresh catalysts in the Top position at 900 °C because the supplied gases firstly react with catalyst in the top position. All catalysts underwent a sharp decrease in weight below 180 °C, which may be due to the loss of adsorbed gas and surface moisture. The weight loss rate of the Cu10/γ-Al_2O_3(70) catalyst after evaporation of the water at temperatures above 180 °C was >100% in the 400–700 °C range. This is because the adsorption of O_2 on the catalyst surface in the process of oxidizing carbon (adsorbed on the catalyst) under air resulted in oxidation of the metal species (Chen et al., 2017). On all alumina carriers, carbon deposition was most noticeable with the inlet (Top) catalyst. High carbon deposition

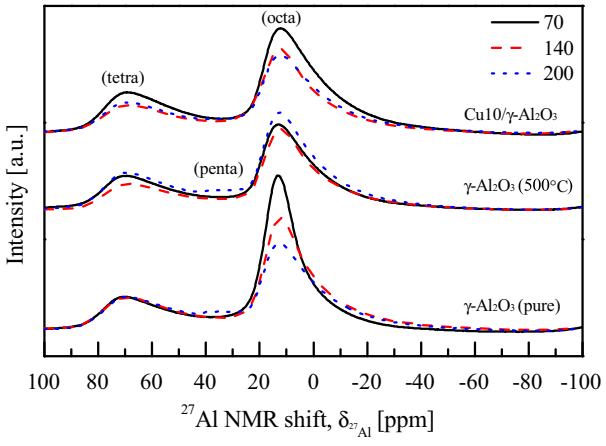

Fig. 8. Solid-state ^{27}Al MAS NMR spectra of Cu10/γ-Al_2O_3 and γ-Al_2O_3.

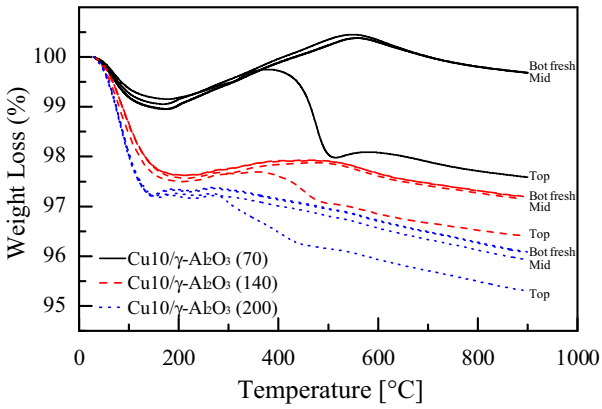

Fig. 9. TGA profiles of Cu10/γ-Al_2O_3 catalysts. (Cu10/γ-Al_2O_3: fresh, Sample location: Top, Mid and Bot).

at the Top position occurs because the concentration of DME/MeOH as coke precursors is higher at this position. During the DME SR reaction, DME hydrolysis (Eq. (2)) and MeOH steam reforming (Eq. (3)) reactions also simultaneously occur. Although MeOH and hydrocarbons could not be analyzed, it is speculated that DME was first converted to MeOH by DME hydrolysis reaction followed by MeOH and DME steam reforming reaction to yield H_2 and CO_2. Concerning the carbon formation, the conversion of MeOH and DME into hydrocarbons can take place on the surface of Cu/Al_2O_3, in particular at the Top positions, and significantly coking may occur by the dehydrogenation of the hydrocarbons (Eq. (10)) due to the lake of oxygen in the supplied gas (Kawabata et al., 2006, Ereña et al., 2013).

$$\text{DME and MeOH} \rightarrow \text{hydrocarbons} \rightarrow \text{dehydrogenation} \rightarrow \text{carbondeposition} \quad (10)$$

At 900 °C in the TGA experiment, the mass of the used catalysts was reduced by 2.1, 0.78, and 0.63% in comparison with that of the fresh catalyst at the Top position. The catalyst with the least carbon deposition was Cu10/γ-Al_2O_3(140) and (200), where this catalyst had the relatively larger BET surface area compared to that of Cu10/γ-Al_2O_3(70).

3.3.2. Time on stream

As seen from the above TGA results, the DME SR catalyst suffers from carbon deposition. Fig. 10 shows the results of time-on-stream (TOS) observation of the reforming characteristics for 12 h. The amount of hydrogen produced was highest during the initial 1.5 h from the beginning of the reaction due to desorbed hydrogen. Thereafter, the SR catalysts were reduced under H_2 atmosphere for 1 h before the experiment. The concentrations of CO generated with the Cu10/γ-Al_2O_3(70) and (140) catalysts were 25 and 20%, respectively, at the beginning of the reaction. However, with both catalysts, the CO concentration reached ~ 25% at 12 h from the beginning of the reaction. The hydrogen produced with Cu10/γ-Al_2O_3(200) (Fig. 10(c)) was very high at the beginning of the reaction and gradually decreased with increasing CO concentration. Finally, the hydrogen production with this catalyst was maintained at 65%, which is higher than that achieved with the other catalysts. DME SR (Eq. (1)) consists as follow: DME hydrolysis to MeOH (Eg. 2), and subsequent MeOH SR to H_2 and CO_2 (Eq. (3)). And other side reactions occur, such as water gas shift reaction (Eq. (4)), DME decomposition (Eq. (5)) and CO or CO_2 methanation (Eq. (9)). CO is produced when DME and MeOH decomposition (Eq. (5) and (7)). As the exposure time increasing in the TOS experiment, the catalytic reaction shifts from DME and MeOH as coke

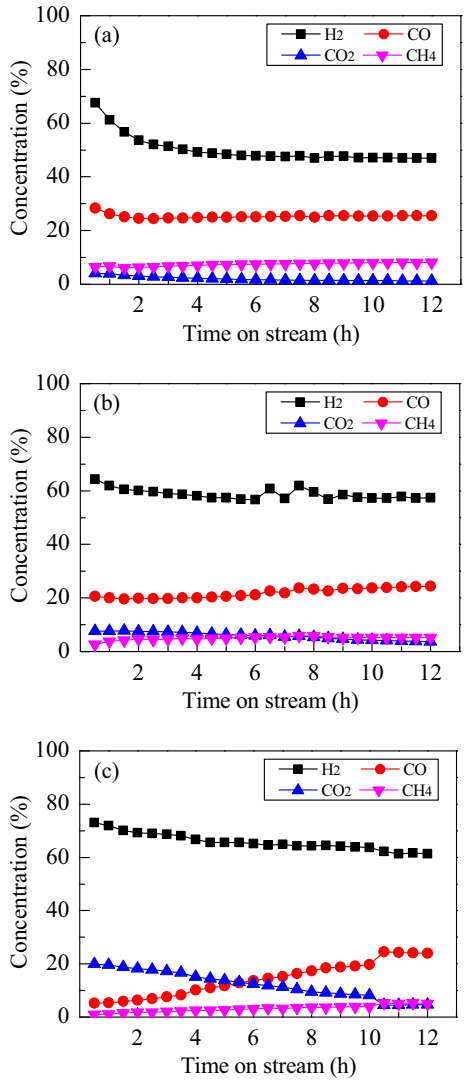

Fig. 10. Time on stream of Cu10/γ-Al_2O_3. (a) Cu10/γ-Al_2O_3(70), (b) Cu10/γ-Al_2O_3(140), (c) Cu10/γ-Al_2O_3 (200). Reforming reaction conditions: S/C ratio: 3, catalyst weight: 5 g, GHSV: 7700 h^{-1}, reaction temperature: 450 °C.

precursors to decomposition reactions, in which CH_4 and CO yield gradually increase and decrease in H_2 yield. In particular, the lowest BET shows sharp drop of H_2 yield compared to BET 140 and 200. This deactivation was caused by DME hydrosis and MeOH decomposition followed by producing CO and CH_4. Furthermore, this deactivation was likely caused by the presence of methoxy species, which is closely related to the formation of carbon residues and CH_4 (Ledesma and Llorca, 2013). In the DME SR reaction, the formation of methoxy ions induced carbon deposition over the catalyst surface because methoxy species are stable and accelerate the catalytic deactivation, which has been previously reported by some researchers (Ledesma and Llorca, 2013, Vicente et al, 2014). Therefore, in the DME SR reaction, the BET of Al_2O_3 affects different coke resistance and durability, in which the lowest BET shows severely deactivation and weak coke resistance compared to BET 140 and 200.

4. Conclusions

The effects of the characteristics of γ-Al_2O_3 on hydrogen production and the stability of the Cu/γ-Al_2O_3 DME SR catalyst were experimentally evaluated. The results of the study are summarized as follows:

The optimum Cu content for maximizing hydrogen production with the Cu/γ-Al_2O_3 DME SR catalyst under the present experimental conditions was 10 wt%. The characteristics of the γ-Al_2O_3 support significantly affected the hydrogen production via the Cu/γ-Al_2O_3 DME SR catalytic reaction. Among the effects, the carbon deposition increased with the amount of CH_4 and CO due to the MeOH and DME as coke precursors, and the catalysts with the least carbon deposition were Cu10/γ-Al_2O_3(200) and (140), which had the relatively large BET surface area compared to Cu10/γ-Al_2O_3(70). The hydrogen production achieved with Cu10/γ-Al_2O_3(200) was up to 72%, which is higher than that of the Cu10/γ-Al_2O_3(70, 140) catalysts. From TGA and TOS evaluation, the BET of Al_2O_3 affects different coke resistance and durability, in which the lowest BET shows severely deactivation and weak coke resistance compared to BET 140 and 200. Cu10/γ-Al_2O_3(200) and (140) catalysts were more durable and stable than Cu10/γ-Al_2O_3(70) due to lower carbon deposition on the catalyst surface.

CRediT authorship contribution statement

Daesuk Kim: Investigation, Resources, Data curation. **Byung-chul Choi:** Conceptualization, Methodology, Validation, Formal analysis, Investigation, Writing - original draft, Writing - review & editing, Visualization, Supervision. **Kyungseok Lee:** Data curation, Writing - review & editing. **Gyeongho Park:** Data curation, Writing - review & editing. **Dong-Weon Lee:** Writing - review & editing. **Seunghun Jung:** Writing - review & editing.

Declaration of Competing Interest

The authors declare that they have no known competing financial interests or personal relationships that could have appeared to influence the work reported in this paper.

Acknowledgements

This research was supported by the Basic Science Research Program through the National Research Foundation of South Korea (NRF) grant funded by the Korea Ministry of Science, ICT & Future Planning (MSIP) (Grant NRF-2015R1A4A1041746).

References

Chen, X., Jiang, J., Li, K., Tian, S., Yan, F., 2017. Energy-efficient biogas reforming process to produce syngas: the enhanced methane conversion by O_2. Appl. Energy 185, 687–697.
Deng, H., Yu, Y., He, H., 2015. Discerning the role of Ag-O-Al entities on Ag/γ-Al_2O_3 surface in NOx selective reduction by ethanol. J. Phys. Chem. C 119, 3132–3142.
Deng, X., Yang, T., Zhang, Q., Chu, Y., Luo, J., Zhang, L., Li, P., 2019. A monolith CuNiFe/γ-Al_2O_3/Al catalyst for steam reforming of dimethyl ether and applied in a microreactor. Int. J. Hydrogen Energy 44, 2417–2425.
Dimethyl ether, 2019. https://en.wikipedia.org/wiki/Dimethyl_ether (accessed 4 September 2019).
Durbin, D.J., Malardier-Jugroot, C., 2013. Review of hydrogen storage techniques for on board vehicle applications. Int. J. Hydrogen Energy 38, 14595–14617.
Elewuwa, F.A., Makkawi, Y.T., 2015. Hydrogen production by steam reforming of DME in a large scale CFB reactor. Part I: Computational model and predictions. Int. J. Hydrogen Energy 40, 15865–15876.
Ereña, J., Vicente, J., Aguayo, A.T., Olazar, M., Bilbao, J., Gayubo, A.G., 2013. Kinetic behaviour of catalysts with different CuO-ZnO-Al_2O_3 metallic function compositions in DME steam reforming in a fluidized bed. Appl. Catal. B Environ. 142–143, 315–322.
Fan, F., Zhang, Q., Wang, X., Ni, Y., Wu, Y., Zhu, Z., 2016. A structured Cu-based/γ-Al_2O_3/Al plate-type catalyst for steam reforming of dimethyl ether: self-activation behavior investigation and stability improvement. Fuel 186, 11–19.
Faungnawakij, K., Fukunaga, T., Kikuchi, R., Eguchi, K., 2008. Deactivation and regeneration behaviors of copper spinel-alumina composite catalysts in steam reforming of dimethyl ether. J. Catal. 256, 37–44.

Fedotov, A.S., Antonov, D.O., Uvarov, V.I., Tsodikov, M.V., 2018. Original hybrid membrane-catalytic reactor for the Co-Production of syngas and ultrapure hydrogen in the processes of dry and steam reforming of methane, ethanol and DME. Int. J. Hydrogen Energy 43, 7046–7054.

Fukunaga, T., Ryumon, N., Shimazu, S., 2008. The influence of metals and acidic oxide species on the steam reforming of dimethyl ether (DME). Appl. Catal. A Gen. 348, 193–200.

Gayubo, A.G., Vicente, J., Ereña, J., Oar-Arteta, L., Azkoiti, M.J., Olazar, M., Bilbao, J., 2014. Causes of deactivation of bifunctional catalysts made up of CuO-ZnO-Al_2O_3 and desilicated HZSM-5 zeolite in DME steam reforming. Appl. Catal. A Gen. 483, 76–84.

González-Gil, R., Herrera, C., Larrubia, M.Á., Kowalik, P., Pieta, I.S., Alemany, L.J., 2016. Hydrogen production by steam reforming of DME over Ni-based catalysts modified with vanadium. Int. J. Hydrogen Energy 41, 19781–19788.

Hwang, H.T., Varma, A., 2014. Hydrogen storage for fuel cell vehicles. Curr. Opin. Chem. Eng. 5, 42–48.

Inagaki, R., Manabe, R., Hisai, Y., Kamite, Y., Yabe, T., Ogo, S., Sekine, Y., 2018. Steam reforming of dimethyl ether promoted by surface protonics in an electric field. Int. J. Hydrogen Energy 43, 14310–14318.

Jiao, Y., Zhang, J., Du, Y., Sun, D., Wang, J., Chen, Y., Lu, J., 2016. Steam reforming of hydrocarbon fuels over M (Fe Co, Ni, Cu, Zn)–Ce bimetal catalysts supported on Al2O3. Int. J. Hydrogen Energy 41, 10473–10482.

Kawabata, T., Matsuoka, H., Shishido, T., Li, D., Tian, Y., Sano, T., Takehira, K., 2006. Steam reforming of dimethyl ether over ZSM-5 coupled with Cu/ZnO/Al_2O_3 catalyst prepared by homogeneous precipitation. Appl Catal A Gen 308, 82–90.

Kwak, J.H., Hu, J.Z., Kim, D.H., Szanyi, J., Peden, C.H., 2007. Penta-coordinated Al^{3+} ions as preferential nucleation sites for BaO on γ-Al_2O_3: An ultra-high-magnetic field ^{27}Al MAS NMR study. J. Catal. 251, 189–194.

Kim, D., Park, G., Choi, B., Kim, Y.-B., 2017. Reaction characteristics of dimethyl ether (DME) steam reforming catalysts for hydrogen production. Int. J. Hydrogen Energy 42, 29210–29221.

Ledesma, C., Ozkan, U.S., Llorca, J., 2011. Hydrogen production by steam reforming of dimethyl ether over Pd-based catalytic monoliths. Appl. Catal. B Environ. 101, 690–697.

Ledesma, C., Llorca, J., 2013. CuZn/ZrO_2 catalytic honeycombs for dimethyl ether steam reforming and autothermal reforming. Fuel 104, 711–716.

Lei, Y., Luo, Y., Li, X., Lu, J., Mei, Z., Peng, W., Chen, R., Chen, K., Chen, D., He, D., 2018. The role of samarium on Cu/Al_2O_3 catalyst in the methanol steam reforming for hydrogen production. Catal. Today 307, 162–168.

Mansouri, A., Khodadadi, A.A., Mortazavi, Y., 2014. Ultra-deep adsorptive desulfurization of a model diesel fuel on regenerable Ni-Cu/γ-Al_2O_3 at low temperatures in absence of hydrogen. J. Hazard. Mater. 271, 120–130.

Manzoli, M., Monte, R.D., Boccuzzi, F., Coluccia, S., Kašpar, J., 2005. CO oxidation over CuOx-CeO_2-ZrO_2 catalysts: Transient behaviour and role of copper clusters in contact with ceria. Appl. Catal. B Environ. 61, 192–205.

Melkozerova, M.A., Gyrdasova, O.I., Baklanova, I.V., Vladimirova, E.V., Zabolotskaya, E.V., Krasil'nikov, V.N., 2018. The effect of preparation method on the defect structure and luminescence properties of γ-Al_2O_3. Mendeleev Commun. 28, 668–670.

Oar-Arteta, L., Remiro, A., Vicente, J., Aguayo, A.T., Bilbao, J., Gayubo, A.G., 2014. Stability of $CuZnOAl_2O_3$/HZSM-5 and $CuFe_2O_4$/HZSM-5 catalysts in dimethyl ether steam reforming operating in reaction–regeneration cycles. Fuel Process. Technol. 126, 145–154.

Oar-Arteta, L., Aguayo, A.T., Remiro, A., Arandia, A., Bilbao, J., Gayubo, A.G., 2016a. Kinetics of the steam reforming of dimethyl ether over $CuFe_2O_4$/γ-Al_2O_3. Chem. Eng. J. 306, 401–412.

Oar-Arteta, L., Remiro, A., Aguayo, A.T., Olazar, M., Bilbao, J., Gayubo, A.G., 2016b. Development of a bifunctional catalyst for dimethyl ether steam reforming with $CuFe_2O_4$ spinel as the metallic function. J. Ind. Eng. Chem. 36, 169–179.

O'Dell, L.A., Savin, S.L.P., Chadwick, A.V., Smith, M.E., 2007. A ^{27}Al MAS NMR study of a sol-gel produced alumina: Identification of the NMR parameters of the θ-Al_2O_3 transition alumina phase. Solid State Nucl. Magn. Reson. 31, 169–173.

Park, S., Kim, H., Choi, B., 2011a. Hydrogen production by steam reforming (SR) of DME over Cu catalysts and de-NOx performance of a combined system of SR + LNT. Catal. Today 164, 240–245.

Park, S., Choi, B., Oh, B.-S., 2011b. A combined system of dimethyl ether (DME) steam reforming and lean NOx trap catalysts to improve NOx reduction in DME engines. Int. J. Hydrogen Energy 36, 6422–6432.

Park, S., Choi, B., Kim, H., Lee, Y.J., 2012. Effective additives to improve hydrothermal aging of DME reforming catalyst in terms of hydrogen yield and de-NOx performance of RC + LNT combined system. Appl Catal A Gen 437–438, 173–183.

Pu, Y.-C., Li, S.-R., Yan, S., Huang, X., Wang, D., Ye, Y.-Y., Lie, Y.-Q., 2019. An improved Cu/ZnO catalyst promoted by Sc_2O_3 for hydrogen production from methanol reforming. Fuel 241, 607–615.

Qin, F., Liu, Y., Qing, S., Hou, X., Gao, Z., 2017. Cu-Al spinel as a sustained release catalyst for H_2 production from methanol steam reforming: Effects of diferent copper sources. J. Fuel Chem. Tech. 45 (12), 1481–1488.

Samain, L., Jaworski, A., Edén, M., Ladd, D.M., Seo, D.-K., Javier Garcia-Garcia, F., Häussermann, U., 2014. Structural analysis of highly porous γ-Al_2O_3. J. Solid State Chem. 217, 1–8.

Semelsberger, T.A., Ott, K.C., Borup, R.L., Greene, H.L., 2006. Generating hydrogen-rich fuel-cell feeds from dimethyl ether (DME) using Cu/Zn supported on various solid-acid substrates. Appl Catal A Gen 309, 210–223.

Takeishi, K., Suzuki, H., 2004. Steam reforming of dimethyl ether. Appl. Catal. A Gen. 260, 111–117.

Takeishi, K., Akaike, Y., 2016. Hydrogen production by dimethyl ether steam reforming over copper alumina catalysts prepared using the sol-gel method. Appl. Catal. A Gen. 510, 20–26.

Tanaka, Y., Kikuchi, R., Takeguchi, T., Eguchi, K., 2005. Steam reforming of dimethyl ether over composite catalysts of γ-Al_2O_3 and Cu-based spinel. Appl. Catal. B Environ. 57, 211–222.

Turco, M., Bagnasco, G., Cammarano, C., Senese, P., Costantino, U., Sisani, M., 2007. Cu/ZnO/Al_2O_3 catalysts for oxidative steam reforming of methanol: the role of Cu and the dispersing oxide matrix. Appl. Catal. B Environ. 77, 46–57.

Thyssen, V.V., Maia, T.A., Assaf, E.M., 2015. Cu and Ni catalysts supported on γ-Al_2O_3 and SiO_2 assessed in glycerol steam reforming reaction. J. Braz. Chem. Soc. 26, 22–31.

Vicente, J., Gayubo, A.G., Ereña, J., Aguayo, A.T., Olazar, M., Bilbao, J., 2013. Improving the DME steam reforming catalyst by alkaline treatment of the HZSM-5 zeolite. Appl. Catal. B Environ. 130–131, 73–83.

Vicente, J., Ereña, J., Oar-Arteta, L., Olazar, M., Bilbao, J., Gayubo, A.G., 2014. Effect of operating conditions on dimethyl ether steam reforming in a fluidized bed reactor with a CuO–ZnO–Al_2O_3 and desilicated ZSM-5 zeolite bifunctional catalyst. Ind. Eng. Chem. Res. 53, 3462–3471.

Vizcaíno, A.J., Carrero, A., Calles, J.A., 2007. Hydrogen production by ethanol steam reforming over Cu-Ni supported catalysts. Int. J. Hydrogen Energy 32, 1450–1461.

Zhang, L., Li, B., Mo, C.-M., Chen, J., 1995. A study of ^{27}Al nuclear magnetic resonace in nanoscale Al_2O_3. NanoStruct. Meter. 5, 299–306.

Zhang, Q., Chu, Y., Deng, X., Zhang, L., Chu, H., 2018a. Improvement of a mesh-type Cu/Ni/γ-Al_2O_3/Al catalyst for steam reforming of dimethyl ether by metal (Fe, Zn or La) addition for CO in situ removal. Mod. Res. Catal. 7, 1–16.

Zhang, T., Ou, K., Jung, S., Choi, B., Kim, Y.B., 2018b. Dynamic analysis of a PEM fuel cell hybrid system with an on-board dimethyl ether (DME) steam reformer (SR). Int. J. Hydrogen Energy 43, 13521–13531.

Zhang, Z., Hu, X., Li, J., Gao, G., Dong, D., Westerhof, R., Hu, S., Xiang, J., Wang, Y., 2018c. Steam reforming of acetic acid over Ni/Al_2O_3catalysts: correlation of nickel loading with properties and catalytic behaviors of the catalysts. Fuel 217, 389–403.